RSC Advances

ROYAL SOCIETY OF CHEMISTRY

www.rsc.org/advances

RSC Advances

ARTICLE

Dietary flavone Chrysin (5, 7-Dihydroxyflavone ChR) functionalized highly-stable metal nanoformulations for improved anticancer applications

Received 00th January 20xx,
Accepted 00th January 20xx

DOI: 10.1039/x0xx00000x

www.rsc.org/

G.Sathishkumar[a], Rashmi Bharti[b], Pradeep K Jha[c], M.Selvakumar[d], Goutam Dey[b], Rakhi Jha[c], M.Jeyaraj[e], Mahitosh Mandal[b] and S.Sivaramakrishnan[a]*

Nanomaterials of noble metals with unique size, shape and composition receives much attention owing to their versatile functionality in personalized cancer nanomedicine. Chrysin (ChR), a natural anticancer bioflavonoid emerged as potential drug therapy for almost all types of cancer, however it has poor solubility and bioavailability. Herein, we report a new approach to formulate biofunctionlized metallic silver (ChR-AgNPs) and gold (ChR-AuNPs) nanoparticles using ChR as direct bioreductant and capping agent. Size and dispersity of nanoparticles (NPs) were controlled through fixing different reaction conditions such as temperature, pH, concentration of metal ion, stochiometric proportion of reaction mixture and incubation time based on their optical properties and SPR effect in UV-visible spectroscopy. Role of hydroxyl and carbonyl groups in functionalizing metal ions with ChR was confirmed with Fourier transform infrared spectroscopy (FTIR) and X-ray photoelectron spectroscopy (XPS) analysis. It also substantiate that oxygen group from ChR donates electron to metal ion and results in complexation, ionic Ag^{+} and Au^{3+} were reduced to Ag^{0} and Au^{0} nano-forms. Physiochemical state of obtained NPs were characterized through different exclusive instrumentation, which shows the presence of highly-stable, spherical, crystalline ChR- AgNPs with the average size of 14±6 nm and 6±2 nm ChR-AuNPs respectively. *In vitro* anticancer results revealed that the formulated metallic NPs exhibits enhanced cytotoxicity than ChR against treated two different breast carcinoma cell lines (MDA-MB-231 and MDA-MB-468). Furthermore, it was evident that NPs cause cell death via induction of apoptosis. Haemolysis assay with human erythrocytes demonstrates good blood biocompatibility of NPs. Thus, the ChR functionalized metal NPs can be potentially employed as combinational drug-nano platform for breast cancer therapy.

1. Introduction

Nano-biotechnology is constantly fast growing research field of the present time which combines biotechnology, nanotechnology, material science, chemical processing and system engineering. It actively engaged in tailoring of new functional nanomaterials with 10^{-9} meter dimension for various industrial and biomedical applications. Interestingly, these dynamic nanomaterials acquire inimitable size, shape and surface properties comparatively to their macroscale counterparts.[1] Recently, a huge attention was given for green synthesis of metal nanoparticles through exploiting different biological entities like bacteria[2], fungi[3], actinomyctes[4], yeast[5], algae[6] and plants.[7] By virtue of their facile, eco-friendly and cost-effective schemes biogenesis was fixed to be most preferred route among other conventional methods.[8] Many studies have demonstrated that the active metabolites such as polyphenols[9], reducing sugars[10] and proteins[11,12] were found to play a key role in reduction and stabilization of nanoparticles (NPs). Interaction of biomolecules with nanomaterials will offer new improved end products. Although, biogenic nanomaterials were found to be an effective contrivance, the actual reduction mechanism and getting narrow size distribution were yet to be clarified.

Over the past decade cancer continues to be a huge burden for mankind, despite the existence of diverse therapeutic strategies. Especially, breast cancer is the most common malignancy among women, incidence rate varied between countries with respect to geography, economic background, life style, age, stage at presentation and biological characteristics.[13] Occurrence of newer breast cancer cases will get two fold increases by the end of 2020.[14] Early detection

[a] Department of Biotechnology and Genetic Engineering, Bharathidasan University, Tiruchirappalli-620024, Tamilnadu, India.
[b] School of Medical Science & Technology, [c] RISUG R&D and Allied Laboratory,
[d] Rubber Technology Centre, Indian Institute of Technology (IIT), Kharagpur - 721302 West Bengal, India.
[e] National Centre for Nanosciences and Nanotechnology, University of Madras, Guindy campus, Chennai 600025, Tamilnadu, India.

Address here.
Corresponding author*
Email: Tel: 0431-2407086: Fax: 0431-2407045
Email: sivaramakrishnan123@yahoo.com (Dr.S.Sivaramakrishnan)
Electronic Supplementary Information (ESI) available: [details of any supplementary information available should be included here]. See DOI: 10.1039/x0xx00000x

and treatment of cancer has been associated with dose-limiting systemic toxicity, prevalence of multiple drug resistance (MDR) and lack of innovative approaches.[15] To overcome these barriers in cancer therapy, recent cutting edge research has been focused on exploring novel therapeutic modalities to combat against breast cancer progression. There are numerous dietary antioxidants like Catechin, Gallocatechin Epicatechin-3-gallate, Epigallocatechin-3-gallate, Apigenin, Genistein, Glycitein, Biochanin A, Formononentin, Quercetin, Kaempferol, Myricetin, Delphinidin, Malvidin and Pelargonidin were explored for cancer prevention.[16] Chrysin (5, 7-dihydroxyflavone), is a natural bioactive dietary flavone abundantly found in honey, passion flowers, *Oroxylum indicum* and propolis. It owns stupendous medicinal properties such as anticancer, anti-inflammatory, antioxidant, hepatoprotective, antimicrobial and anti-diabetic effects. Also, it is now well established that ChR inhibits cancer cell growth through induction of apoptosis, cell cycle arrest, inhibition of angiogenesis, invasion and metastasis without adverse side effects to normal cells.[17] While ChR was proposed to be an extraordinary chemotherapeutic agent, it always suffers with lot of efficacy limitations like poor solubility and bioavailability.[18] An ideal nanoparticulate system of noble metals, polymers and other inorganic materials can improve target-specificity, porosity, solubility and increased bioavailability of various chemotherapeutic agents.[19]

The large surface area to volume ratio and different structural properties of nano-drugs would target tumour sites by a passive process. Also, arrangement of leaky vasculature and poor lymphatic drainage of cancer cells will leads to enhanced permeability and retention (EPR) effect. Materials at nano scale level can easily pass through the cellular barriers and strongly interacts with functional biomolecules.[20] Ultimately, it will offer many biomedical insights for clinical level applications.

Noble metal NPs such as gold, silver, copper, platinum, palladium, iron, zinc and titanium have gained colossal attention due to their indispensable applications in drug delivery[21], imaging[22], Surface-Enhanced Raman Scattering (SERS) detection[23], antioxidant[24], anti-inflammatory[25], bactericidal[26] and cancer theranostics.[27] Metal-flavonoid complexes have elicited great interest in recent years for their potential therapeutic applications. In an attempt to further improve the anticancer efficacy of ChR, we used this flavone as instant reductant to generate functionalized highly-stable AgNPs and AuNPs. Most importantly it reveals the reduction mechanism and kinetics of biogenesis of nanomaterials (Scheme 1). On the other hand, *in vitro* anticancer studies demonstrate the enhanced chemotherapeutic potential of formulated NPs for breast cancer therapy.

2.0. Experimental section

2.1. Materials

Silver nitrate ($AgNO_3$), Chloroauric acid ($HAuCl_4$), Chrysin (5, 7-dihydroxyflavone), 3-(4, 5-dimethyl- 2-thiazolyl)-2, 5-diphenyl-2H-tetrazolium bromide (MTT), Heat inactivated fetal calf serum (FBS), minimum essential medium (MEM), glutamine, EDTA and trypsin were purchased from Sigma–Aldrich (St. Louis, USA). All glasswares were washed with distilled water followed by acetone and dried in oven before use. Breast cancer cell lines MDA-MB-231 and MDA-MB-468 were obtained from National Centre for Cell Science (NCCS), Pune, India.

2.2. Size controlled synthesis of ChR-AgNPs and ChR-AuNPs

In typical synthesis process, the reaction mixture was prepared by adding 12mg of ChR in 100 ml of metal ion (1 mmol/L) solution under constant stirring. The pH was adjusted with 0.1 N NaOH and 0.1 N HCl to reach to reach different pH ranging (5, 6, 7, 8, 9 and 10). Temperature was controlled using a thermostat magnetic stirrer (37°C, 50 °C, 60 °C, 70 °C, 80 °C, 90 °C and 100 °C). Concentration of metal ion $AgNO_3$ & $HAuCl_4$ (0.5, 1, 1.5, 2 and 3 mM), concentration of ChR (0.5, 1, 1.5 and 2mM), stochiometric proportion of metal ion/ChR (1:1, 1:2, 1:3, 1:4 and 2:1) and incubation time (0-60 minutes) were fixed. The optimal conditions will get control over the nucleation and growth of the NPs with better size distribution. Influence of these parameters on size, shape and yield of the NPs were studied preliminarily through SPR absorbance spectra in UV-Visible spectrometer.

2.3. Characterization of ChR-AgNPs and ChR-AuNPs

Reduction of $AgNO_3$ and $HAucl_4$ were monitored by UV-Visible spectrophotometer based on SPR of all the reaction parameters. Before, high throughput characterization the colloidal NPs suspensions were purified by dialysis using a cellulose tube (MWcutoff 12 400 D) against 1 L of deionized water for 24 h at 30° C to remove excess metal ion and unreacted ChR. To perform UV-Vis, a small aliquot of sample was diluted with distilled water and absorbance maxima were scanned by Perkin-Elmer Lambda 2 UV198 UV-Visible Spectrophotometer, at the wavelength of 300–700 nm. FTIR spectroscopic measurements was carried out to study the surface chemistry of NPs, samples were mixed with KBr powder and pelletized after drying the transmittance were recorded using JASCO 460 PLUS FTIR spectrometer (Wavelength range between 4000 cm^{-1} to 400 cm^{-1}). X-ray diffraction (XRD) was performed to determine the dimension of synthesized NPs with h, k, l values. The diffraction pattern was obtained with conditions at 40 kV and 30 mA in Cu, Ka radiation and mean particles size (L) (PAN analytical X pert PRO Model) of NPs were calculated using following Debye-Scherrrer's equation.

$$L = 0.9\lambda/\beta \cos h\, \theta$$

Where, λ is the wavelength of X-ray, β is full width and half maximum and θ is the Bragg's angle. The surface oxidation state and presence of element in the sample were studied using XPS. It was carried out using an omicron ESCA spectrometer with monochromatized Al Kα radiation. Morphology of nanoparticles was studied using the images

obtained with high resolution transmission electron microscope (HRTEM). To perform TEM analysis, purified NPs solution were allowed for sonication for 10-20min, a drop of this solution was used to make a thin layer on copper coated grid and allowed to dry. The micrographs were taken at different magnification using JEOL JEM 2100 HRTEM operating at 100Kev. Energy-dispersive X-ray spectroscopy (EDS or EDX or EDAX) is an analytical technique used for elemental analysis or chemical characterization of sample. EDX spectra and selected area diffraction (SEAD) pattern of NPs were obtained along with HRTEM (JEOL JEM 2100) analysis. Size distribution and surface charge of synthesized NPs were measured using dynamic light scattering (DLS) and zeta potential analyzer (Malvern Zetasizer, Nano-ZS90). Concentrations of formulated NPs were measured with inductively coupled plasma atomic emission spectroscopy (ICP-OES Perkin–Elmer Optima 5300 DV model).

2.4. *In vitro* anticancer studies

2.4.1. Cell lines

The MDA-MB-468 and MDA-MB-231 cells were cultured in Dulbecco's Modified Eagle's Medium: Nutrient Mixture F-12 (Ham) (D-MEM/ F-12) with 15 mM HEPES buffer, L-glutamine, pyridoxine hydrochloride, supplemented with 1.2 g Sodium bicarbonate (Invitrogen Corporation, CA), antibiotics (10,000 U/L penicillin and 10 mg/L streptomycin) (Himedia, Mumbai, Maharashtra India) and 10% fetal bovine serum (FBS) (Invitrogen, Grand Island, NY, USA). Cells were incubated at 37°C in a 5% CO_2 and 95% humidified incubator.

2.4.2. Cell viability analysis (MTT Assay)

Cytotoxicity of NPs were measured using MTT (3-(4, 5-dimethylthiazol-2-yl)-2, 5- diphenyl tetrazolium bromide) assay.[28] Briefly, cells in their exponential growth phase were trypsinized and seeded in 96-well flat-bottom culture plates at a density of 1×10^4 cells per well in 100 µL of complete Dulbecco's modified eagle's medium (DMEM). Then, cells were allowed to adhere and grow for 24h at 37°C in the presence of 5% CO_2. After 24h, the medium was replaced with 100 µL fresh incomplete DMEM medium containing different concentrations of ChR (0, 5, 10, 20, 25, 50, 75, 100, 150 and 200 µg/ml), ChR-AgNPs and ChR-AuNPs (0, 2, 5, 10, 15, 20, 25, 30, 40 and 50 µg/ml) and incubated for 48 h at 37°C in 5% CO_2. At the end of incubation, fresh media containing 0.40 mg/mL MTT were added to the 95-well plates and incubated for another 4h at 37°C in 5% CO_2. The formazan crystals formed after 4h were solubilized in 100 µl of DMSO after aspirating the medium. The absorbance was monitored at 595 nm using a 96-well plate reader (Bio-Rad, Hercules, CA, USA). Growth inhibition was determined using:

Growth inhibition = (control O.D.-sample O.D.)/control O.D.

The IC_{50} value was defined as the concentration of NPs that produced a 50% reduction of cell viability.

2.4.3. Analysis of Apoptosis (TUNEL assay)

The level of apoptosis induced by ChR and formulated NPs were identified via a terminal deoxynucleotidyl transferase (TdT)-mediated dUTP nick end labelling (TUNEL) staining using the *in Situ* Cell Death Detection Kit–Fluorescein (Roche Molecular Biochemicals, Chemicon Int., Temecula, CA, USA) as per manufacturer's instructions. Briefly, cells were grown on poly-L-lysine-coated glass cover slips and treated with ChR, ChR-AgNPs and ChR-AuNPs for 48 hours. Subsequently, the medium was removed and slides were washed three times with PBS (pH 7.4), fixed with 4% paraformaldehyde in PBS (pH 7.4) and permeabilized with 0.1% Triton X-100. Aliquots (50 mL) of the reaction mixtures were applied to cover slides and placed in a humidified incubator at 37°C for 60 minutes. After incubation, cells were washed with PBS, air dried and mounted on slides. Finally, the slides were examined by epi-fluorescence microscopy.[29]

2.4.4. Hemocompatibility assay

Hemocompatibility assay was performed as per the earlier report[30] with slight modification. The samples ChR, ChR-AgNPs and ChR-AuNPs were individually suspended in 10 mM HEPES buffer saline. Fresh blood was collected from healthy volunteers in sterile lithium heparin vacutainers. Red blood cells (RBCs) were separated by centrifugation (1500 rpm for 10 min at 4°C) and a ficoll density gradient. RBCs were further diluted in 20 mM HEPES buffered saline (pH 7.4) to 5% v/v solution. The RBC suspension was added to HEPES saline, 1% Triton X- 100 and samples at different concentration of ChR (2, 5, 7 and 9 µg/ml), ChR-AgNPs and ChR-AuNPs (10, 20, 30 and 40 µg/ml) and incubated at 37°C for 30 and 60 min. All samples were prepared in triplicate and after being slightly vortexed the suspension was incubated at static conditions for 4h at 37°C. After incubation, all the samples were centrifuged (Heraeus table top centrifuge 5805R, Germany) at 12,000 rpm at 4°C and supernatants were transferred to a 96-well plate. The hemolytic activity was determined by measuring the absorbance at 570 nm (Biorad microplate reader model 550, Japan). Control samples of 0% lysis (in HEPES buffer) and 100% lysis (in 1% Triton X-100) were employed in the experiment. The percent of hemolysis was calculated as follows:

Hemolysis % = [(sample absorbance - negative control)/ (positive control - negative control)] 100%.

This study was approved by the Institutional ethics committee (IEC) of Bharathidasan University (Ref No. DM/2014/101/54).

3.0. Result and Discussion

Generation of metallic Ag and Au nanostructures by reduction of $AgNO_3$ and $HAucl_4$ with chrysin was initially confirmed through the formation of yellowish brown and ruby red colour respectively. Fig. 1a1 & b1 shows variation in colour intensity of ChR-AgNPs and ChR-AuNPs synthesized at different ChR concentration attributes SPR phenomenon, which relies on size, shape and dispersity of nanopartiles.[31, 32]. The preliminary results revealed that ChR can be used as a direct bioreductant

to fabricate AgNPs and AuNPs without addition of any other toxic chemical ingredient.

3.1. Size controlled synthesis of ChR-AgNPs and ChR-AuNPs

As mentioned earlier, after blending ChR with metal ions the reaction mixture exhibits variations in colour due to excitation of Surface Plasmon Resonance (SPR), formation of yellowish brown colour and ruby red colour indicates the synthesis of ChR-AgNPs and ChR-AuNPs. The optimal reaction mixture to synthesis monodispersed stable nanomaterials was fixed as 0.5 mM ChR and 1mM metal ions in 1:2 ratio (Fig. S1a, b and c & Fig. S2a, b and c Supporting Information). NPs generated at this stochiometric proportion generates intense SPR spectra which clearly denotes the presence of smaller nanoparticles, whereas the other precursor concentration produces broad and weaker SPR peak due to increased polydispersity.[33] As per, LaMer model it was envisaged that formation of NPs could only happen when the precursor concentration is within a suitable range for nucleation. However, this range might vary amongst different biomass-assisted synthesis approaches. Dubey et al., 2010 observed that NPs synthesized at higher metal ion concentration were larger and red shift occurred in SPR spectra as an indicative of polydispersity.[34]

Likewise, physiological parameters such as temperature and pH mainly influence the synthesis of NPs. Increasing the temperature (37°C to 100°C) reflects in the nucleation growth of NPs. Synthesis was found higher at 90°C when compared to other temperature, ChR-AgNPs and ChR-AuNPs synthesized at 90°C shows SPR peak at 420 nm & 530 nm (Figure S1d & Figure S2d Supporting Information). Above 90°C the SPR peak was observed at lower wavelength regions due to reduced size range of NPs and they were found unstable. It was believed that lesser synthesis of NPs occurred at lower temperature because of the plasmon band was not accompanied with a significant increase in intensity at lower temperature.[35] Increasing the temperature reflects in SPR peak, at higher temperature rate of NPs synthesis reaching maximal point which shows intense absorbance peak relatively to the size of NPs.[36]

pH of the reaction medium plays a crucial role in metal ion reduction, from our results it was inferred that, in alkaline pH-9 (Fig. S1e Supporting Information) the synthesis of ChR-AgNPs was found higher. In alkaline pH, the aggregation of NPs was believed to be favoured over the nucleation to form narrow size nanoparticles.[37] On the other hand, stable ChR-AuNPs were formed at acidic pH-6 (Fig. S2e Supporting Information), it generates an intense SPR peak at 530 nm. Usually, biosorption mechanism of Au is ionic rather than covalent due to the dependence of Au binding with pH. At lower pH, gold is present in solution in anionic form ($AuCl_4$) and the functional groups of active biocompounds on the biomass surface such as hydroxyl groups tend to undergo protonation and become positively charged. The overall positively charged surface could promote the interaction between protonated functional groups and the negatively charged ($AuCl_4$) through electrostatic attraction or electrovalent bond.[38] As a result, biosorption was preferred over bioreduction of Au ions. The bioreduction of gold could occur through the oxidation of hydroxyl to carbonyl groups. The pH of the colloid is lowered in most cases after the synthesis completed. Our study, the complete reduction of metal ion was noticed after 60min incubation time, yield of NPs was direct proportion with reaction time. Similarly, Dwivedi et al., 2010 reported that the peak absorbance was sharper when the contact time was increased at 2h time duration.[39] As compared to previous reports our synthesis method requires much shorter time which can be useful for easy scaling up process.

3.2. Characterization of ChR-AgNPs and ChR-AuNPs

Generally, noble metal NPs were known to exhibit SPR phenomenon where conducting electrons of metals oscillate collectively in resonance with certain wavelengths upon interaction with an electromagnetic field. These SPR band highly depends on type, size, shape of the NPs and surrounding environment.[40] UV-visible spectroscopy displays intense SPR peak at 420 nm for ChR-AgNPs and 530 nm for ChR-AuNPs (Fig. 1c & d) respectively, the synthesized NPs were stable at room temperature even after 45 days. The IR spectrum of free ChR manifests prominent transmittance located at 3080, 3009, 2945, 1655 and 1610 cm−1 (Fig. 2). The strong bands between 3500-3000 cm−1 corresponds to the O-H stretch whereas 1655 and 1610 cm−1 attributes C=O and C=C respectively. The characteristic IR transmittance of synthesized NPs clearly implicates that functional groups of ChR actively participates in coordination with metal ions. Variations in the intensity of transmittance at 3500-3000 cm-1 noticed in formulated ChR-NPs complex which clearly depicts the symmetrical and asymmetrical stretching modes of O-H undergoes changes after the reduction. This difference in intensity suggests the loss of one O-H group during the coordination to the metal ions.[41] A strong band at about 1655 cm-1 detected in the transmittance of ligand is assigned to C=O which was shifted to 1638 cm-1 in the spectra of ChR-NPs complex which denotes that functionalization of ChR on metal NPs occurs through the C=O oxygen atom.[42]

XRD pattern of ChR-AgNPs and ChR-AuNPs were interpreted with JCPDS intensitives, after reduction the diffraction peaks at 2θ = 38.03◦, 46.18◦ and 63.43◦ were indexed as (1 1 1), (2 0 0) and (2 2 0) planes of a faced centered cubic (fcc) lattice of silver (JCPDS, file no. 04-0783) (Fig. 3a1). The XRD patterns displayed here are consistent with earlier reports.[43] Likewise, for AuNPs the XRD peak corresponding to four peaks (JCPDS, No. 89−3722) at (38.17˚), (44.36˚) and (64.65˚) (Fig. 3b1) which are found to be an identical with those reported for the standard gold metal (Au˚).[44] The mean size of ChR-AgNPs and ChR-AuNPs was calculated using Debye–Scherrer's equation by determining the width of (1 1 1) peak and found to be 15 and 8 nm respectively which is fairly in agreement with the HRTEM measurement.

Fig. 3a2 & b2 displays the XPS general scan spectrum of ChR-AgNPs and ChR-AuNPs which shows the presence of strong C1s, O1s, Ag3d and Au4d core levels accordingly. The strong

signal of Ag 3d (370 eV) and Au4f (87.5 eV) indicates the presence of Ag and Au metal. The C 1s peak observed at a binding energy of ~285 eV serves as a reference to correct the binding energy NPs. shift and it also stems from ChR to coordinate. The spectrum also consists of O (~531 eV) elements in their respective binding energy positions due to the interaction of ChR with synthesized NPs. Thus, it was concluded from XPS measurements that the metal ions were reduced to nano metallic form, and the NPs were capped by ChR.[24,42] HRTEM micrographs display the fine configuration of uniform size spherical ChR-AgNPs with mean size of 14±6 nm (Figure 4a). Interestingly, Au colloid displays both spherical and oval-shaped NPs with an average size of 6±2 nm (Fig. 5a). It was also found that both ChR-AgNPs and ChR-AuNPs having a thin layer of ChR coating on its surface, particles were well dispersed and stable for long period of time. There is no direct contact of particles were noticed, it's mainly due to the presence capping agent.[45] Higher magnification TEM micrographs exposes excellent crystallinity of NPs, the distance of 0.23 nm between lattice planes is in agreement with the (1 1 1) lattice spacing of face centered cubic (fcc) Ag (d111 = 0.2359 nm) and Au (0.235 nm). Crystalline nature of the NPs was further evidenced by the SAED pattern (Fig. 3(d)). Clear lattice fringes in high-resolution TEM image and the typical SAED pattern (Fig. 4b & 5b) with bright circular rings corresponds to (1 1 1), (2 0 0), (2 2 0), (3 1 1) and (2 2 2) planes indicates that the synthesized NPs are highly crystalline.[42] EADX spectra display a strong metal peak for Ag and Au, the presence of copper is due to copper grid used for the HRTEM-analysis (Fig. S3a & b). The hydrodynamic diameter of ChR- Ag and AuNPs were evaluated by DLS which confirms the particle size distribution respectively (Fig. 4c & 5c), their corresponding zeta potential value is suggesting high stability of NPs (Fig. S4a & b). The large negative potential value could be due to the capping agent, which generate repulsive forces between the NPs.[46] ICP-OES results specifies the concentration of synthesized NPs were quantified to be 65.89 & 103.3 mg/L of ChR-AgNPs and ChR-AuNPs in that order. It denotes that more than 80% of the metal ions have been reduced to nano scale values.

3.3. *Invitro* anticancer studies

3.3.1. Analysis of cell viability (MTT assay)

Cell viability assay clearly explains the cellular response to a toxicant, in our study synthesized NPs exhibits higher anticancer activity than ChR. There was a dose-dependent cellular toxicity was observed in ChR (0, 5, 10, 20, 25, 50, 75, 100, 150 and 200 µg/ml), synthesized ChR-AgNPs and ChR-AuNPs (0, 5, 10, 20, 30, 40, and 50 µg/ml) treated MDA-MB-468 and MDA-MB-231 breast cancer cell lines. ChR-AgNPs gives more cytotoxic effect (IC50-15 µg/ml & 12 µg/ml) followed by ChR-AuNPs (IC50- 19 µg/ml & 21 µg/ml) (Fig. 6 a1 & b1) and ChR (IC50- 72 µg/ml & 35 µg/ml) (Figure 6 a2 & b2) against treated MDA-MB-468 and MDA-MB-231 breast cancer cell lines. Especially, the cytotoxicity effect of formulated NPs were much stronger than free ChR, depicts the improved anticancer efficacy of ChR after getting functionalized with Ag and Au nanostructures. The NPs size, shape, surface area and surface functionalization are major factors that influence biokinetics and toxicity.[47] It should be mentioned that the concentration of synthesized NPs used in this case was very less when compared to ChR. This decrease in cell viability with increase in NPs concentration, suggests that more number of NPs could accumulate inside cells resulting in enhanced stress, ultimately leading to cell death. These results clearly specify the enhanced effectiveness of the ChR functionalized NPs against cancer cells. It was demonstrated in our earlier study that AgNPs synthesized using phamolocolgically important *Dendrophthoe falcata* with a size range of 5–45 nm has shown enhanced cytotoxicity against human breast carcinoma cells (MCF-7) compared to the aqueous plant extract.[37] Similarly, Selim and Hendi (2012) reported the toxic responses of AuNPs to human breast epithelial MCF-7 cells, they noticed the cytotoxicity effect of AuNPs on MCF-7 cells and apoptotic response in dose depended manner.[48]

3.3.2. Analysis of apoptosis (TUNEL assay)

Apoptosis is the key event in cancer therapy that can be measured with the activation caspase-cascade, chromatin aggregation, partition of cytoplasm and nucleus into membrane-bound vesicles (apoptotic bodies) which contain ribosomes, morphologically intact mitochondria, and nuclear material.[49] We performed TUNEL staining to identify apoptotic cell death induced by ChR, synthesized ChR-AgNPs and ChR-AuNPs. TUNEL-positive nuclei were found throughout the photomicrographs of the treated groups but few in untreated controls, and numbers of positive nuclei increased with treatment time (Fig. 7a &b). Previous references have showed that the possible mechanism involved in the AgNPs induced cellular toxicity begin with the cellular uptake of inorganic nanoparticles through clathrin-dependent endocytosis and macropinocytosis.[50]

Inorganic NPs profoundly interact with cells and intracellular macromolecules like proteins and DNA.[51] Cellular uptake of NPs leads to generation of reactive oxygen species which provoke oxidative stress. It is clearly evidenced that synthesized NPs (both Ag and Au) induces cell damage through loss of cell membrane integrity, oxidative stress and apoptosis. Several factors influences toxicity of NPs such as dose, time and size of the particles and it was found that biogenic AgNPs and AuNPs shows does and time dependent toxicity against HeLa cells.[52,53] It was discussed that biologically synthesized AgNPs cause cellular damage in Hep-2 cell line through induction of oxidative stress.[54] Recently several studies have shown that AgNPs trigger intracellular ROS by inhibiting the synthesis of intracellular antioxidant systems. The generated ROS favors the DNA damage leading to cell death, Piao et al., reported that highly reactive hydroxyl radicals released by AgNPs causes damage to cellular components including DNA.[55] According to the earlier study, it was documented that AgNPs functionalized with plant phenolics induce oxidative stress that

leads to apoptosis via mitochondria-dependent and caspase-mediated pathways.[52]

3.3.3. Hemocompitibility assay

Hemocompitibility of ChR, synthesized ChR-AgNPs and ChR-AuNPs were assessed upon measuring the damage to human RBCs. Our result shows that synthesized NPs exhibits comparatively lower red haemoglobin release than ChR. Fig. 8 a & b are photographs of the RBCs exposed to ChR-AgNPs, ChR-AuNPs and free ChR at different concentrations. As shown in Fig. 8, compared to positive control and ChR the haemolytic activity of NPs was less considerable, implying its safe nature in application. The mechanisms of direct haemolytic activity for different toxic agents were found to be non-specific. Especially, the plant derived xenobiotic compounds such as phenols, are capable of promoting haemolysis through oxidation of haemoglobin, forming metahemoglobin.[56] Our data highly corroborate with Ruden et al[57] who reported that silver nanoparticles did not show haemolytic activity against erythrocytes even at the higher concentrations (up to 1024 µg/mL). In another report, AuNPs synthesized using *Z. officinale* extract have shown high level compatibility with the blood cells which do not initiates any aggregation of cells and also the NPs do not seem to activate the platelets. It was inferred that surface passivation of nanomaterials with different bio agents will improve their biocompatibility.[58] Eventually, this can be easily used for different biological applications, which require them as vehicles for drug release. Moreover, as per the International Organization for Standardization/Technical Report 7406, the haemolysis admissible level of bio-based materials was 5%. The exposure of ChR functionalized metallic nanomaterials shows meagre level of haemolysis, revealing their biocompatibility and suitability for biomedical applications.

Conclusions

Natural anticancer flavone ChR (5, 7-Dihydroxyflavone ChR) has been used to synthesis AgNPs and AuNPs in greener route without toxic additives. ChR strongly reduces Ag^{+} and Au^{3+} into their nano-forms with uniform size, shapes and surface chemistry. Size and dispersity of nanoparticles were controlled by changing different reaction conditions. It was observed that metal ions strongly absorbs ChR via hydroxyl group and functionalize them for improved stability. Formulated NPs have shown tremendous anticancer activity against breast carcinoma cells, NPs triggers cellular toxicity via apoptosis. Compare to free ChR synthesized NPs gives improved anticancer action, depicts the enhanced solubility, bioavailabity and durability of ChR after functionalized with NPs. In contrast, ChR capped NPs shows less haemolytic activity than ChR portrays its biocompatibity nature. This opens up several possibilities for ChR-NPs to be used as an appropriate therapeutic approach to save breast cancer patient's life. Further studies are in progress to implicate the molecular mechanism and metabolic pathways involved in cellular apoptosis.

References

1. J. Huang, Q. Li, D. Sun, Y. Lu, Y. Su, X. Yang, H. Wang, Y. Wang, W. Shao, N. He, J. Hong and C. Chen, *Nanotechnology*, 2007, **18**, 1.
2. T. Klaus, R. Joerger, E. Olsson and C. Granqvist, *PNAS*, 1999, **96**, 13611.
3. P. Mukherjee, A. Ahmad, D. Mandal, S. Senapati, S.R. Sainkar, M.I. Khan, R. Ramani, R. Parischa, P. V. Ajayakumar, M. Alam, M. Sastry and R. Kumar, *Angew. Chem. Int. Ed*., 2001, **40**, 3585.
4. A. Ahmad, S. Senapati, M.I. Khan, R. Kumar and M. Sastry, *Langmuir*, 2003, **19**, 3550
5. M. Kowshik, S. Ashtaputre, S. Kharrazi, W. Vogel, J. Urban , S.K. Kulkarni and K.M. Paknikar, *Nanotechnology*, 2003, **14**, 95.
6. J. Xie, J.Y. Lee, D.I.C. Wang and Y.P. Ting, *ACS Nano*, 2007, **1**, 429.
7. G.Sathishkumar, C. Gobinath, K. Karpagam, V. Hemamalini, K. Premkumar and S. Sivaramakrishnan, *Colloids and Surfaces B: Biointerfaces*, 2012, **95**, 235
8. K.B.Narayanan and N. Sakthivel, *Advances in Colloid and Interface Science*, 2011, **169**, 59.
9. N. Ahmad, S. Sharma, Md.K. Alam, V.N. Singh, S.F. Shamsi, B.R. Mehta and A. Fatm, *Colloids and Surfaces B: Biointerfaces*, 2010, **81**, 81.
10. M. Sathishkumar, K. Sneha and Y.S. Yun, *Bioresource Technology*, 2010, **101**, 7958.
11. N. Muniyappan and N.S. Nagarajan, *Process Biochemistry*, 2014, **49**, 1054.
12. C. Rajkuberan, K. Sudha, G. Sathishkumar and S. Sivaramakrishnan, *Spectrochimica Acta Part A: Molecular and Biomolecular Spectroscopy*, 2015, **136**, 924.
13. D.M. Parkin, F.Bray, J. Ferlay and P.Pisani, *CA Cancer J Clin*., 2005, **5**, 574.
14. F. Brayand and B. Moller, *Nat. Rev. Cancer*, 2006, **6**, 63.
15. P. Parhi, C. Mohanty and S.K. Sahoo, *Drug Discovery*, 2012 **17**, 1044.
16. H. Yao, W. Xu, X. Shi and Z. Zhang, *Journal of Environmental Science and Health*, Part C, 2011, **29**, 1.
17. E.R. Kasala, L.N. Bodduluru, R.M. Madana, K.V. Athira, R.Gogoi and C.C. Barua. *Toxicol Lett.*, 2015, **233**, 214.
18. S. Chakraborty, S. Basu, A. Lahiri and S. Basak, *Journal of Molecular Structure*, 2010, **977**, 180.
19. S. Dawar1, N. Singh, R.K. Kanwar, R.L. Kennedy, R.N. Veedu, S.F. Zhou, S. Krishnakumar, S. Hazra, S. Sasidharan, W. Duan and J.R. Kanwar, *Drug Discovery Today*, 2013, **18**, 1292.
20. M.S. Bhojani, M.V. Dort, A. Rehemtulla and B.D. Ross, *Molecular Pharmaceutics*, 2010, **7**, 1921.
21. Y.Q. Du, X.X. Yang, W.L. Li, J. Wang and C.Z. Huang, *RSC Adv.*, 2014, **4**, 34830.
22. X. Huang, I.H.E. Sayed, W. Qian and M.A.E. Sayed, *J. Am. Chem. Soc.*, 2006, **128**, 2115.
23. W. Cai, T. Gao, H. Hong and J. Sun, *Nanotechnol. Sci. Appl.*, 2008, 1
24. D.K. Singh, R. Jagannathan, P. Khandelwal, P.M. Abraham and P. Poddar, *RSC Nanoscale*, 2013, **5**, 1882.
25. L. David, B. Moldovan, A. Vulcu, L. Olenic, M.P. Schrepler, E.F. Fodor, A. Florea, M. Crisan, I. Chiorean, S. Clichici and G.A. Filip, *Colloids and Surfaces B: Biointerfaces*, 2014, **122**, 767.
26. K. Chaloupka, Y, Malam and A.M. Seifalian, *Trends Biotechnol.*, 2010, **28**, 580.
27. S. Mukherjee, D. Chowdhury, R. Kotcherlakota, S. Patra, B. Vinothkumar, M.P. Bhadra, B. Sreedhar and C.R. Patra, *Theranostics*, 2014, **4**, 316.

28. T. Mosmann, *J. Immunol. Methods.*, 1983, **65**, 55.
29. S.K. Jaganathan, A. Mazumdar, D. Mondhe and M. Mandal, *Cell Biol. Int.*, 2011, **35**, 607.
30. P. Venkatesan, N. Puvvada, R. Dash, B.N.P. Kumar, D. Sarkar, B. Azab, A. Pathak, S.C. Kundu, P.B. Fisher, M. Mandal, *Biomaterials*, 2011, **32**, 3794.
31. J.J. Mock, M. Barbic, D.R. Smith, D.A. Schultz, and S.Schultz, *J. Chem. Phys.*, 2002, **116**, 6755.
32. K. Kwon, K.Y. Lee, Y.W. Lee, M. Kim, J. Heo, S.J. Ahn and S.W. Han, J. Phys. Chem. C, 2007, **111**, 1161.
33. Q. Guo, Q. Guo, J. Yuan and J. Zeng, *Colloids and Surfaces A: Physicochem. Eng. Aspects*, 2014, **441**, 127.
34. S.P. Dubey, M. Lahtinen, M. Sillanpaaa, Process Biochemistry, 2010, **45**, 1065.
35. J.Y. Song and B.S. Kim, *Bioprocess Biosyst. Eng.*, 2009, **32**, 79.
36. A. Rai, A. Singh, A. Ahmad and M. Sastry, *Langmuir*, 2006, **22**, 736.
37. G. Sathishkumar, C. Gobinath, A. Wilson and S. Sivaramakrishnan, *Spectrochimica Acta Part A: Molecular and Biomolecular Spectroscopy*, 2014, **128**, 285.
38. Y. Zhou, W. Lin, J. Huang, W. Wang, Y. Gao, L. Lin, Q. Li, L. Lin and M. Du, *Nanoscale Res. Lett.*, 2010, **5**, 1351.
39. A.D. Dwivedi and K. Gopal, *Colloids and Surfaces A: Physicochem. Eng. Aspects*, 2010, **369**, 27.
40. S.S. Shankar, A. Rai, A. Ahmad and M. Sastry, *J Colloid Interface Sci.*, 2004, **275**, 496.
41. J. Kasthuri, S. Veerapandian and N. Rajendiran, *Colloids and Surfaces B: Biointerfaces* 2009, **68**, 55.
42. S. Li, Y. Shen, A. Xie, X. Yu, L. Qiu, L. Zhang and Q. Zhang, *Green Chem.*, 2007, **9**, 852.
43. D. Philip, C. Unni, S.A. Aromal and V.K. Vidhu, *Spectrochimica Acta Part A: Molecular and Biomolecular Spectroscopy*, 2011, **78**, 899.
44. D. Philip, *Spectrochimica Acta Part A: Molecular and Biomolecular Spectroscopy*, 2009, **73**, 374.
45. C. Krishnaraj, E.G. Jagan, S. Rajasekar, P. Selvakumar, P.T. Kalaichelvan and N. Mohan, *Colloids and Surfaces B: Biointerfaces*, 2010, **76**, 50.
46. T.J.I. Edison and M.G. Sethuraman, *Process Biochemistry* 2012, **47**, 1351.
47. A. Nel, T. Xia, L. Madler and N. Li, *Science*, 2006, **311**, 622.
48. M.E. Selim and A.A. Hendi, *Asian Pacific Journal of Cancer Prevention*, 2012, **13**, 1617.
49. M. Jeyaraj, A. Renganathan, G, Sathishkumar, A. Ganapathi and K. Premkumar, *RSC Adv.*, 2015, **5**, 2159.
50. C. Greulich, J. Diendorf, T. Simon, G. Eggeler, M. Epple and M. Koller, *Acta Biomaterialia* 2011, **7**, 347.
51. P.V. AshaRani, G.L. KahMun, M.P. Hande and S. Valiyaveettil, *ACS Nano*, 2009, **3**, 279.
52. M. Jeyaraj, M. Rajesh, R. Arunb, D. MubarakAli, G. Sathishkumar, G. Sivanandhan, G.K. Dev, M. Manickavasagam, K. Premkumar, N. Thajuddin and A. Ganapathi, *Colloids and Surfaces B: Biointerfaces* 2013, **102**, 708– 717.
53. M. Jeyaraj, R. Arun, G. Sathishkumar, D. MubarakAli, M. Rajesh, G. Sivanandhan, G. Kapildev, M. Manickavasagam, N. Thajuddin and A. Ganapathi, *Materials Research Bulletin*, 2014, **52**, 15.
54. S. Kim, J.E. Choi, J. Choi, K.H. Chung, K. Park, J. Yie and D.Y. Ryu, *Toxicology in Vitro*, 2009, **23**, 1076.
55. M.J. Piao, K.A. Kang, I.K. Lee, H.S. Kim, S. Kim, J.Y. Choi, J. Choi and J.W. Hyun. *Toxicol Lett.*, 2011, **201**, 92.
56. S. Selvaraj, S. Krishnaswamy, V. Devashya, S. Sethuraman and U.M. Krishnan, *Langmuir*, 2011, **27**, 13374
57. S. Ruden, K. Hilpert, M. Berditsch, P. Wadhwani and A.S. Ulrich, *Antimicrob. Agents Chemother.*, 2009, **53**, 3538.
58. K.P. Kumar, W. Paul and C.P. Sharma, *Process Biochemistry*, 2011, **46**, 2007.

Schematic Diagram 1

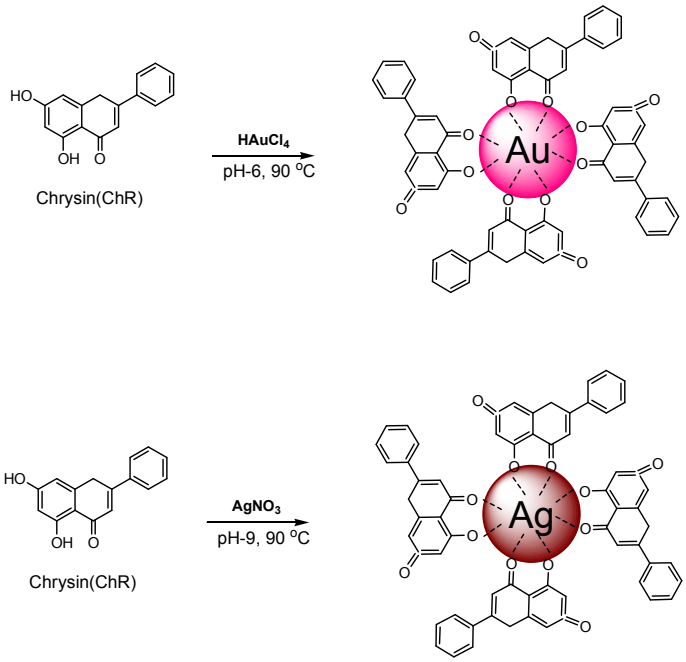

Scheme 1 Illustration of reduction and functionalization of AgNPs and AuNPs using Chrysin (ChR) as direct bioreductant

Fig. 1

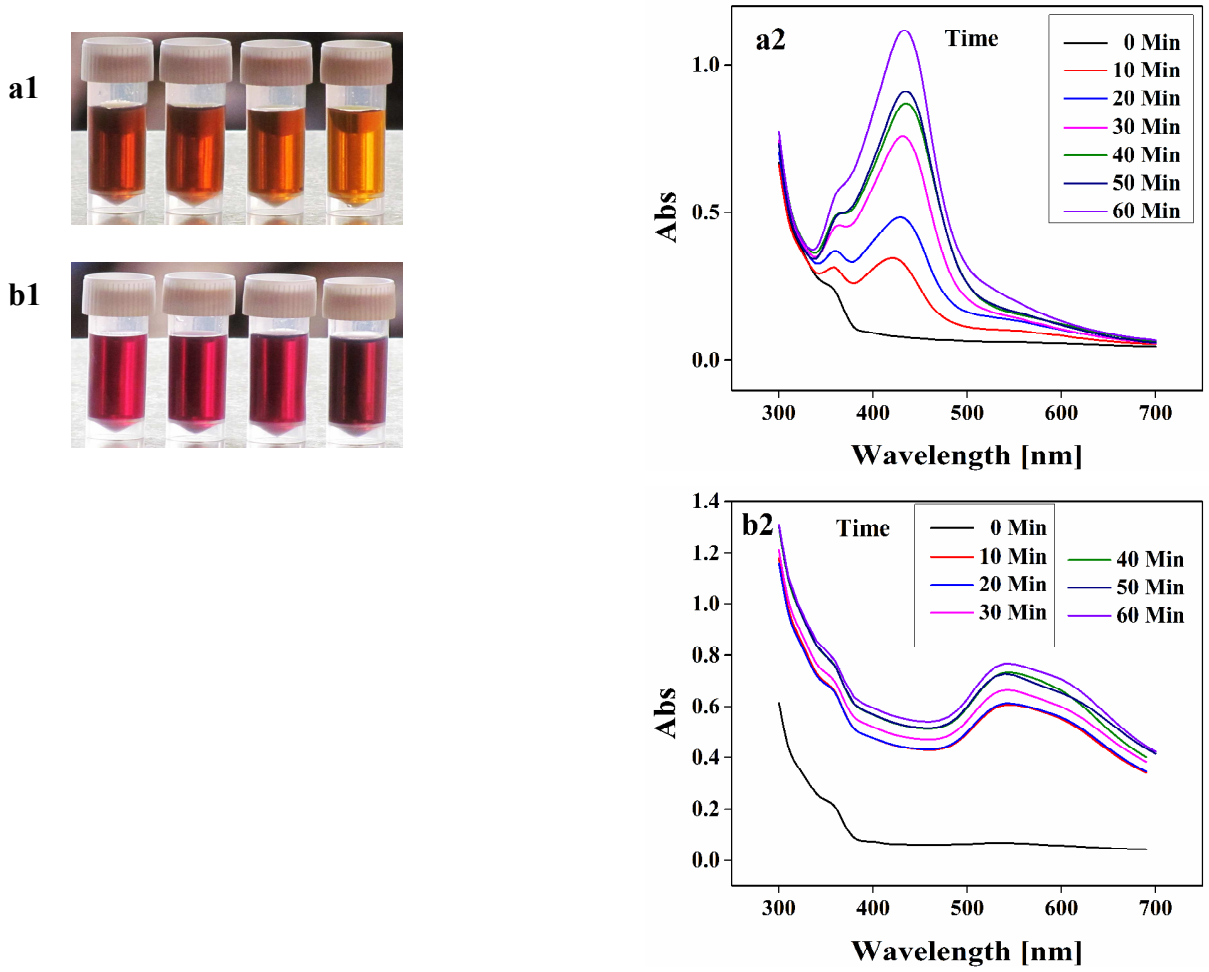

Fig. 1 Color intensity pattern of ChR-AgNPs and ChR-AuNPs synthesized at different concentration of ChR from 0.5 mM to 2 mM **(a1)** Formation of yellowish brown color and **(b1)** ruby red color due to excitation SPR indicates the generation of ChR-AgNPs and ChR-AuNPs respectively. **(a2 & b2)** shows the absorbance UV-Vis spectroscopy analysis of ChR-AgNPs and ChR-AuNPs which displays an intense SPR spectra at 420nm and 530 nm.

Fig. 2

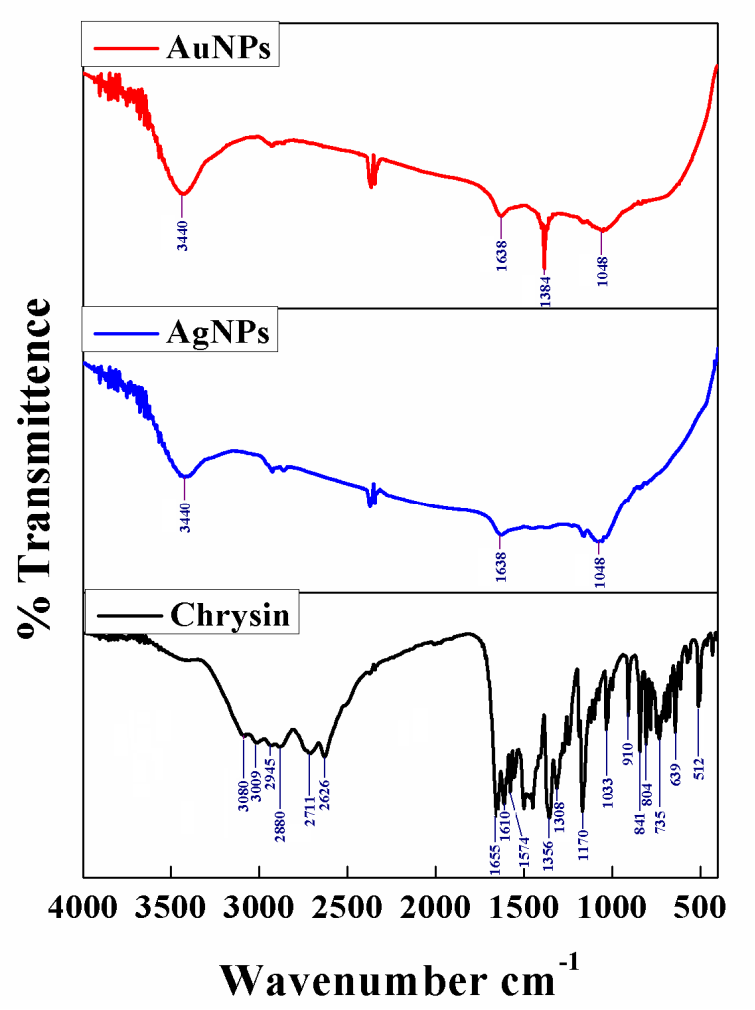

Fig. 2 FTIR transmittance shows the surface absorption of ChR by metal ions, it strongly confirms the role hydroxyl (O-H) and carbonyl (C-=O) functional group of ChR in reduction and stabilization of NPs.

Fig. 3

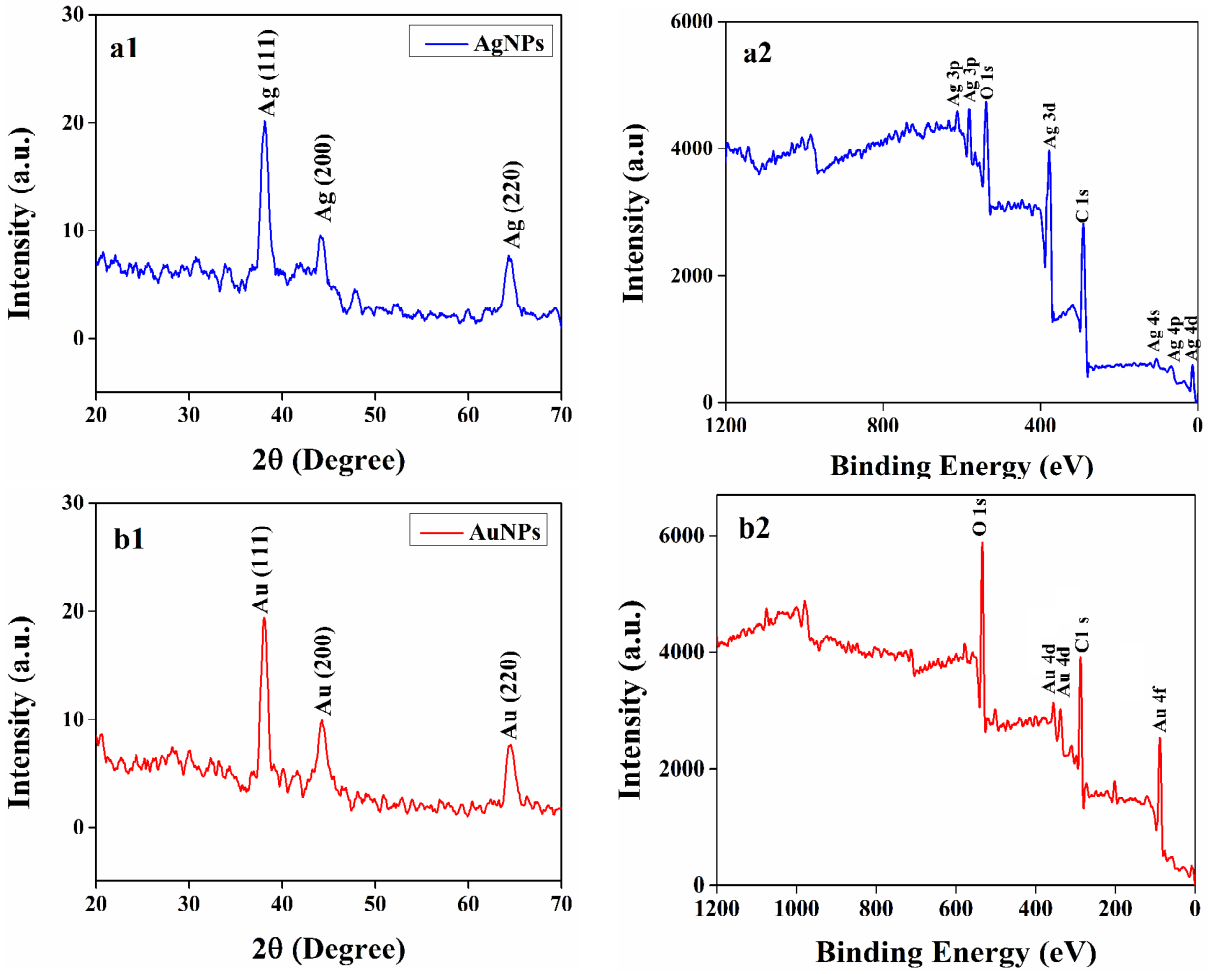

Fig. 3 XRD pattern of synthesized ChR-AgNPs and ChR-AuNPs (a1 & b1) shows the diffraction index for face centered cubic (Fcc) silver (Ag) and gold (Au). XPs survey of (a) ChR-AgNPs and (b) ChR-AuNPs

Fig. 4

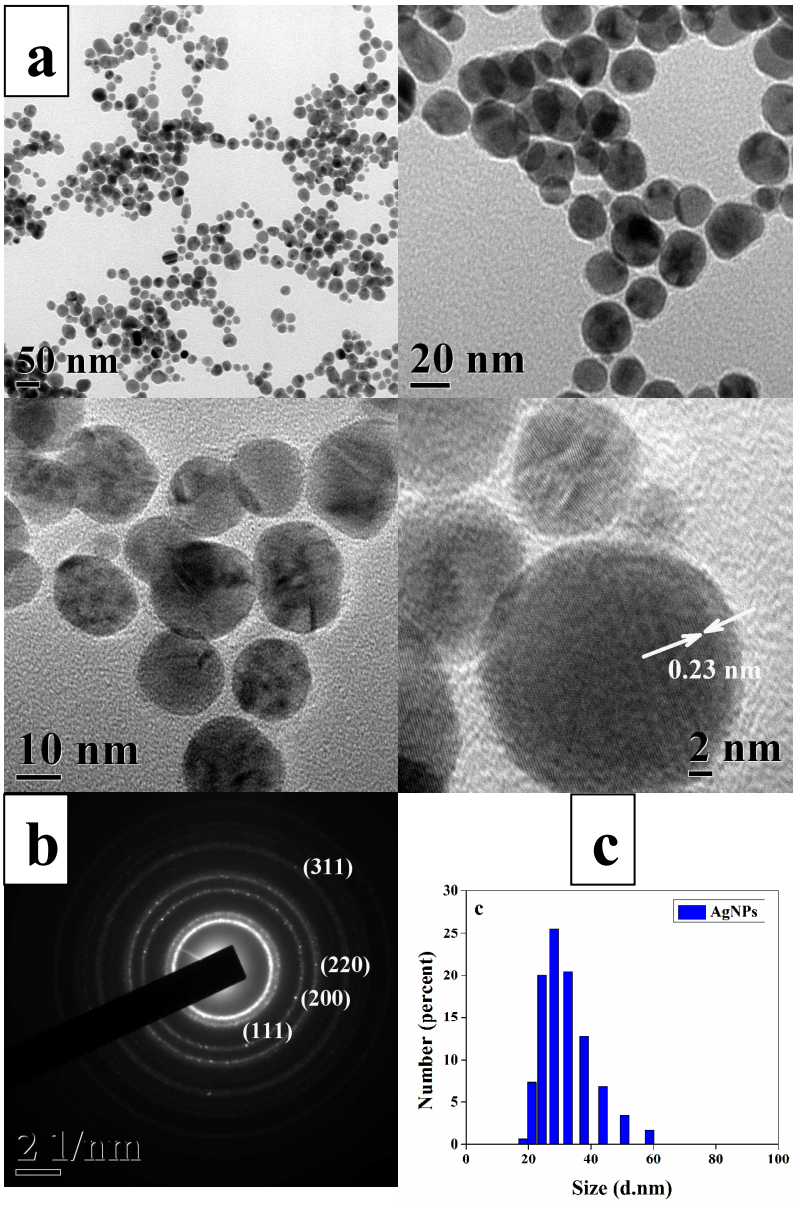

Fig. 4 HRTEM micrographs of ChR-AgNPs s (a) Well dispersed spherical-shaped ChR-AgNPs with the average of 14±6 nm, high-magnified image of single nanocrystal showing lattice fringes with spacing of 0.23 nm and (b) SAED pattern (c) DLS particle size distribution pattern.

Fig. 5

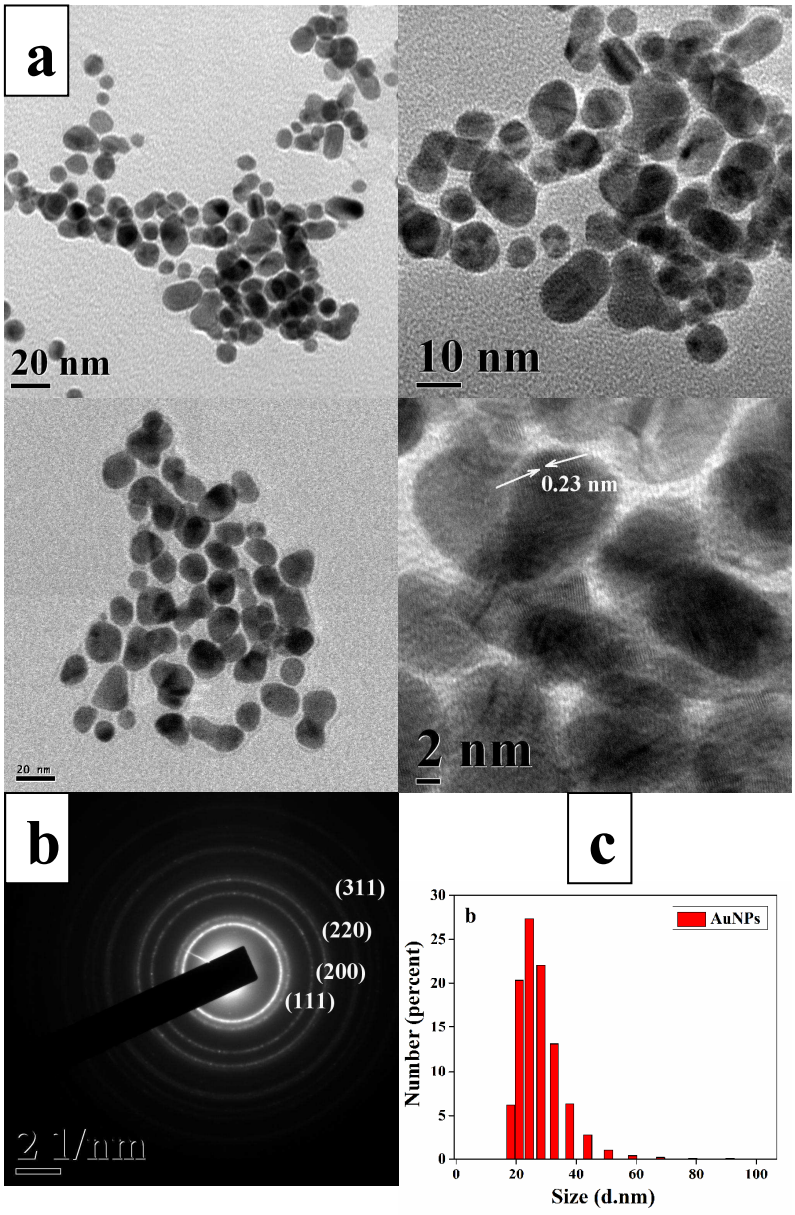

Fig. 5 HRTEM micrographs of ChR-AuNPs (a) Well dispersed spherical and oval-shaped ChR-AuNPs with average size of 6±2 nm, high-magnified image of single nanocrystal showing lattice fringes with spacing of 0.23 nm and (b) SAED pattern (c) DLS particle size distribution pattern.

Fig. 6

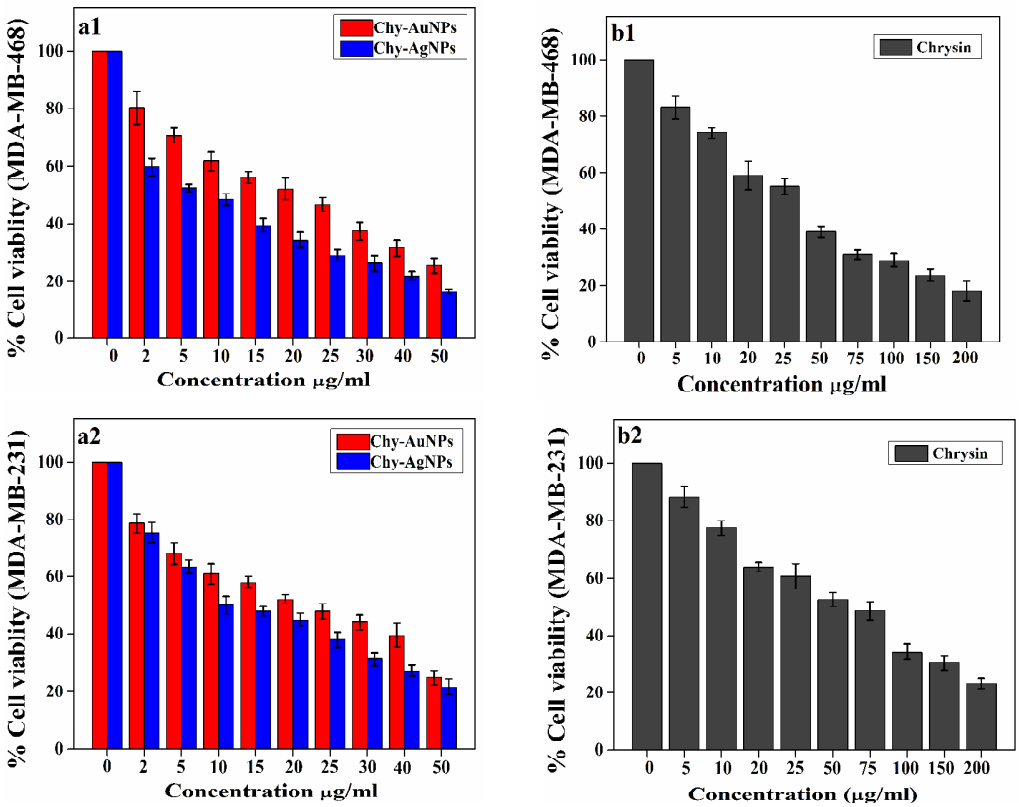

Fig. 6 *In vitro* anti proliferative assay by MTT reagent in MDA-MB-468 and MDA-MB-231. (a1 and b1) Formulated ChR-AgNPs, ChR-AuNPs and (b1 and b2) free ChR were given at different doses for 48 h. All the data are expressed as the mean±SD of the three experiments with duplicate wells.

Fig. 7

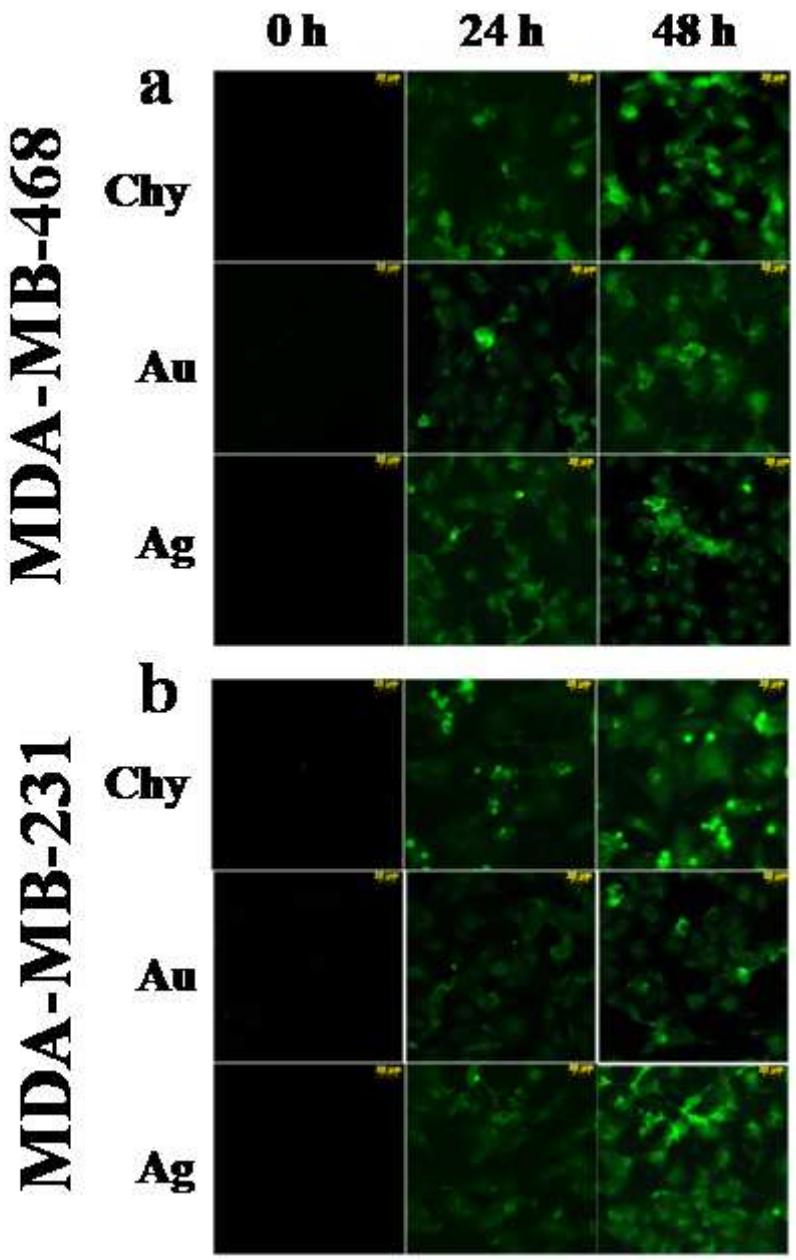

Fig. 7 Induction of apoptosis by formulated ChR-AgNPs, ChR-AuNPs and free ChR were measured through TUNNEL assay in treated (a) MDA-MB-468 and (b) MDA-MB-231 breast carcinoma cell lines. Epi-fluorescence microscopic image shows apoptotic cells (TUNEL-positive nuclei) at different incubation time intervals (24 h and 48h).

Fig. 8

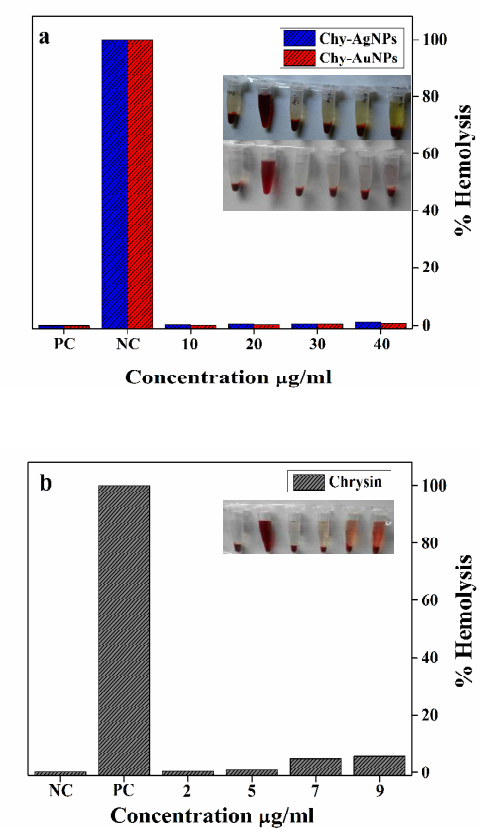

Fig. 8 *Invitro* hemocompatibility assay of **(**a) formulated ChR-AgNPs, ChR-AuNPs and (b) Free ChR. Nil (0%) lysis was noticed in negative control (NC-HEPES buffer) whereas positive control (PC- 1% Triton X-100) shows 100% lysis. Formulated NPs exhibits very less hemolytic activity than free ChR.